Title

Codelivery of synergistic antimicrobials with polyelectrolyte nanocomplexes to treat bacterial biofilms and lung infections.

Authors

Finbloom, Joel
Raghavan, Preethi
Kwon, Michael
et al.

Codelivery of synergistic antimicrobials with polyelectrolyte nanocomplexes to treat bacterial biofilms and lung infections

Joel A. Finbloom[1,2]*, Preethi Raghavan[1], Michael Kwon[3], Bhushan N. Kharbikar[1], Michelle A. Yu[3]*, Tejal A. Desai[1,4]*

Bacterial biofilm infections, particularly those of *Pseudomonas aeruginosa* (PA), have high rates of antimicrobial tolerance and are commonly found in chronic wound and cystic fibrosis lung infections. Combination therapeutics that act synergistically can overcome antimicrobial tolerance; however, the delivery of multiple therapeutics at relevant dosages remains a challenge. We therefore developed a nanoscale drug carrier for antimicrobial codelivery by combining approaches from polyelectrolyte nanocomplex (NC) formation and layer-by-layer electrostatic self-assembly. This strategy led to NC drug carriers loaded with tobramycin antibiotics and antimicrobial silver nanoparticles (AgTob-NCs). AgTob-NCs displayed synergistic enhancements in antimicrobial activity against both planktonic and biofilm PA cultures, with positively charged NCs outperforming negatively charged formulations. NCs were evaluated in mouse models of lung infection, leading to reduced bacterial burden and improved survival outcomes. This approach therefore shows promise for nanoscale therapeutic codelivery to treat recalcitrant bacterial infections.

INTRODUCTION

Antimicrobial resistance (AMR) is a global health crisis recognized by the Centers for Disease Control and Prevention and the World Health Organization as a dire threat to human health. Increasing rates of antimicrobial resistant and tolerant bacterial infections are outcompeting the development of new antibiotics, and deaths from bacterial infections are estimated to increase to more than 10,000,000 annual deaths by 2050 (*1*). A major mechanism of antimicrobial tolerance in bacterial infections is the development of biofilms, where bacteria encase themselves within heterogeneous biological hydrogels of extracellular DNA, polysaccharides, and protein filaments (*2*). Biofilm formation directly increases bacterial virulence and leads to antimicrobial tolerance mechanisms such as limited antibiotic penetration and increased expression of efflux pumps (*2–4*). Bacterial biofilms are estimated to occur in up to 80% of human infections and can be 1000 times more tolerant to antibiotics when compared to planktonic bacteria (*2*). Biofilm infections are particularly prevalent within chronic wounds such as diabetic skin ulcers and in lung infections of patients with cystic fibrosis (CF). In the lungs of patients with CF, the viscous mucus layer caused by ineffective mucus clearance by epithelial cells poses an additional challenging barrier to effective bacterial treatment (*5*). Patients with CF are thus chronically colonized by bacterial infections, particularly those of *Pseudomonas aeruginosa* (PA) bacteria, which, once established, are nearly impossible to eradicate even in the era of CF transmembrane conductance regulator modulators (*6–8*). Chronic colonization by PA greatly affects the morbidity and mortality of patients with CF, requiring continuous

month-long courses of inhaled tobramycin (Tob) and aztreonam antibiotics to prevent pathologic PA strains from developing into exacerbations. If an acute-on-chronic exacerbation due to PA arises, then patients with CF may require double coverage with two intravenous antibiotics of distinct classes for 2 weeks, increasing vulnerability to developing colonization with AMR bacteria.

The codelivery of synergistic antimicrobial drugs could improve the treatment of AMR bacterial infections and help eradicate persistent chronic infections (*9–11*). These drug combinations can function in parallel to target orthogonal mechanisms and prevent the evolution of resistance pathways. Combination therapeutics can also work together to enhance a singular pathway, such as by facilitating increased uptake of an antibiotic for improved efficacy (*12, 13*). One particularly promising combination of antimicrobial therapeutics is Tob and silver nanoparticles (AgNPs). Tob is an aminoglycoside antibiotic that is the backbone of most antibiotic therapies used in CF exacerbations due to PA. Several studies have demonstrated that Tob and AgNPs act synergistically to overcome antibiotic tolerance within PA biofilms (*14–17*). While the exact mechanism of action has not yet been elucidated, it is hypothesized that AgNPs inhibit biofilm formation, increase membrane permeability for enhanced Tob uptake, and generate reactive oxygen species for direct bactericidal activities. Despite its potential, one major challenge to antimicrobial codelivery is maintaining local therapeutic concentrations of both drugs at the same site of infection, particularly if the site is difficult to reach. This results in immense burdens for patients who are frequently exposed to prolonged courses of antibiotics at potent doses, which increases patients' risk for developing adverse reactions and AMR (*5*). In colonized patients with CF, inhaled Tob and aztreonam are effective in reducing exacerbations due to PA; however, these therapies require dosing two to three times a day, which encumber patients' ability to attend work and school. In chronic osteomyelitis, a duration of 2 to 6 weeks of parenteral antibiotics followed by 4 to 8

[1]Department of Bioengineering and Therapeutic Sciences, University of California, San Francisco, San Francisco, CA, USA. [2]Faculty of Pharmaceutical Sciences, University of British Columbia, Vancouver, BC, Canada. [3]Division of Pulmonary and Critical Care Medicine, University of California, San Francisco, San Francisco, CA, USA. [4]School of Engineering, Brown University, Providence, RI, USA.
*Corresponding author. Email: joel.finbloom@ubc.ca (J.A.F.); michelle.yu2@ucsf.edu (M.A.Y.); tejal_desai@brown.edu (T.A.D.)

additional weeks of oral antibiotics is required, and even then, the infections often persist (18). Therefore, approaches are needed to enable therapeutic codelivery, improve antimicrobial efficacies, and overcome tolerant bacterial biofilm infections.

Nanoparticle-based strategies for antimicrobial delivery have seen early preclinical success in sustained drug release and treating bacterial infections (19–26). Polymeric particles are widely used as nanoscale drug carriers for antimicrobial delivery, as they can be fabricated from biocompatible polymers, loaded with bioactive cargo, and delivered via inhalation (27, 28). In addition, polymeric particles have tunable properties such as size, shape, surface charge, and polymer composition, which can influence particle biodistribution, half-life, and interactions with biological barriers such as mucus and bacterial biofilms (29–33). Polyelectrolyte nanocomplexes (NCs) are an emerging class of polymeric nanoparticle drug carrier and are formed through electrostatic interactions between oppositely charged components (34, 35). These NC drug carriers offer physicochemical tunability dependent on the polymer ratios, chemical structures, pK_a values (where K_a is the acid dissociation constant), and molecular weights (34). NCs have further advantages in their ease of fabrication without specialized equipment and in their high loading efficiencies of therapeutic cargos, especially for drugs of high charge densities (35, 36), which often have low encapsulation efficiencies (ee%) using other polymeric systems (37). However, NC formulations for the codelivery of synergistic antimicrobials remain a challenge, as it is difficult to load diverse classes of cargo within a single NC drug carrier.

To enable the codelivery of Tob and AgNP antimicrobials to treat PA lung infections, we developed a nanoscale drug carrier fabrication platform that combines approaches from polyelectrolyte nanocomplexation and layer-by-layer (LbL) electrostatic self-assembly. This NC-LbL strategy led to the formation of NCs coloaded with Tob and AgNPs (Fig. 1A). These AgTob-NCs were fabricated

from commercially available materials without the use of any specialized equipment. In addition, AgTob-NCs offer tunability in particle size and surface charge to engineer the drug carrier biointerface and enhance antimicrobial activity. AgTob-NCs had high degrees of loading for both Tob (>75%) and AgNPs (>95%) and facilitated the codelivery of Tob and AgNP antimicrobials to enhance antimicrobial activity against PA biofilms that were tolerant to either treatment alone. AgTob-NCs demonstrated potency in vivo in reducing bacterial burden and improving survival outcomes in mouse models of acute PA lung infection. This approach could see widespread use in enabling the codelivery of diverse classes of antimicrobials to overcome recalcitrant bacterial infections.

RESULTS
Tob NC fabrication and characterization

To fabricate NCs coloaded with Tob and AgNPs, NCs were first optimized to encapsulate Tob alone, followed by electrostatic LbL self-assembly with AgNPs (Fig. 1A). Tob is an aminoglycoside antibiotic with five potential sites for amine protonation (Fig. 1B) and is therefore well suited for electrostatic incorporation into polyelectrolyte NCs. Dextran sulfate (DS) was chosen as the complementary negatively charged polymer to form Tob-NCs, as its polysaccharide structure and dense negative charge (Fig. 1C) make it ideal for complexation with positively charged Tob. Tob and DS were coincubated together to form NCs, which were characterized for drug ee % as well as particle size and surface charge by dynamic light scattering (DLS) and zeta potential measurements, respectively (Fig. 2A).

NC formation conditions were optimized for pH and buffer type, with optimal conditions observed using 50 mM sodium acetate buffer at pH 4. This pH allowed for increased protonation of Tob amines while maintaining a DS-negative charge. Tob and DS coincubation at pH 4 demonstrated increased particle formation when compared to pH 6, wherein no Tob encapsulation or particle formation was observed. Using these optimized conditions, we observed Tob:DS ratio–dependent trends in particle size, surface charge, and Tob ee% (Fig. 2D). A mass ratio of 1:1 Tob:DS led to microparticles of positive charge that were highly polydisperse and had low Tob ee% of 39%. As the ratio of Tob:DS increased to 1:2, an increase in ee% was observed at 86%; however, the particles were of ~1.4 μm in diameter, likely too large to penetrate efficiently through bacterial biofilm hydrogels, which have reported mesh sizes on the order of hundreds of nanometers (29, 38). At Tob:DS ratios of 1:3 and 1:4, 250- to 300-nm particles were formed, with ee% at 58 (1:3) and 57% (1:4). Thus, Tob-NC **1c**, corresponding to a Tob:DS ratio of 1:3, was chosen for subsequent AgNP loading and antimicrobial studies, as this NC formulation matched reported biofilm porosities and had acceptable levels of Tob loading.

AgTob-NC fabrication and characterization

Tob-NCs **1b** to **1d** displayed strong negative charges (Fig. 2A) due to the mass ratios of <1 Tob:DS within the particles. Because AgNPs also have a negatively charged surface because of their citrate coatings, we used an LbL self-assembly approach to cofunctionalizing NCs with both Tob and AgNPs. LbL approaches have been used extensively in the field of drug delivery and nanoparticle functionalization, although predominantly with thin films and non–NC-formulated polymeric particles (25, 39–41). Commercially available
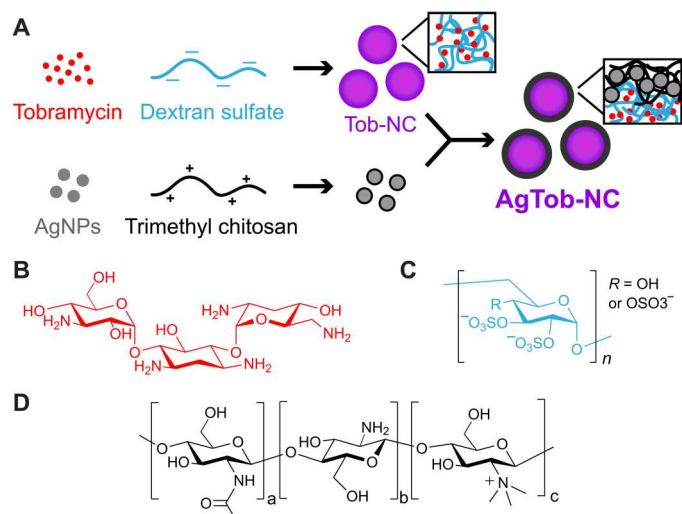

Fig. 1. Polyelectrolyte NC formation coupled with LbL assembly enables the codelivery of antimicrobials to treat bacterial infections. (**A**) Complexation of Tob (positive charge) with dextran sulfate (DS) polymers (negative charge) led to the formation of NCs. The LbL addition of trimethyl chitosan (TMC) and AgNPs facilitated the coloading of antimicrobials onto NCs. Chemical structures of (**B**) Tob, (**C**) DS, and (**D**) TMC. TMC contains units of chitin, chitosan, and TMC within the polymer, with TMC being the dominant unit.

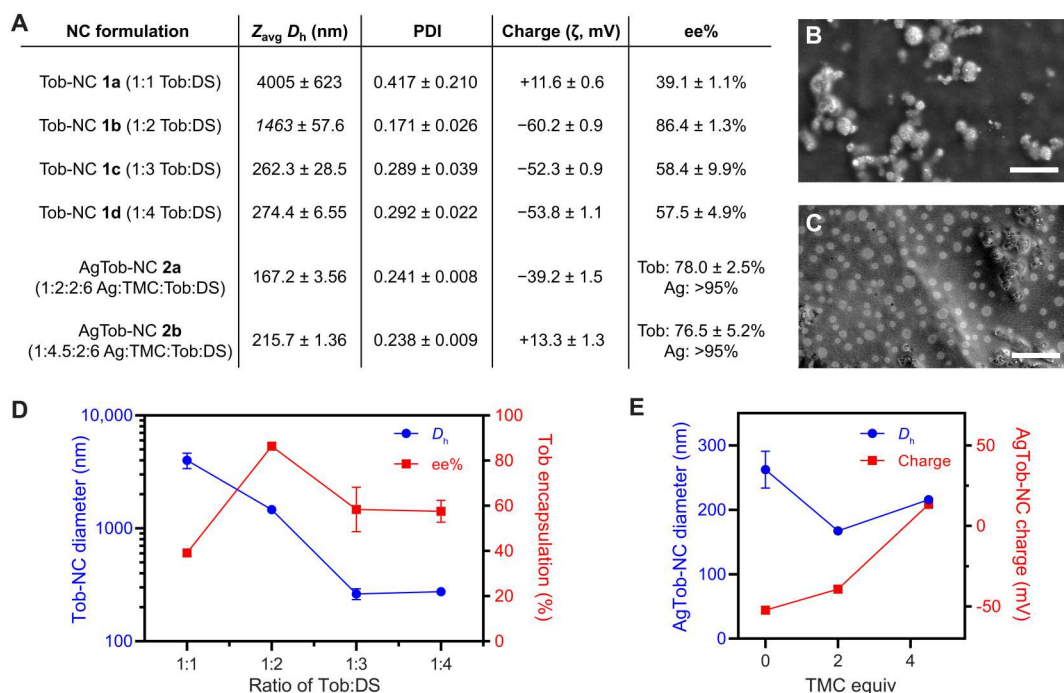| NC formulation	Z_{avg} D_h (nm)	PDI	Charge (ζ, mV)	ee%
Tob-NC **1a** (1:1 Tob:DS)	4005 ± 623	0.417 ± 0.210	+11.6 ± 0.6	39.1 ± 1.1%
Tob-NC **1b** (1:2 Tob:DS)	*1463* ± 57.6	0.171 ± 0.026	−60.2 ± 0.9	86.4 ± 1.3%
Tob-NC **1c** (1:3 Tob:DS)	262.3 ± 28.5	0.289 ± 0.039	−52.3 ± 0.9	58.4 ± 9.9%
Tob-NC **1d** (1:4 Tob:DS)	274.4 ± 6.55	0.292 ± 0.022	−53.8 ± 1.1	57.5 ± 4.9%
AgTob-NC **2a** (1:2:2:6 Ag:TMC:Tob:DS)	167.2 ± 3.56	0.241 ± 0.008	−39.2 ± 1.5	Tob: 78.0 ± 2.5% Ag: >95%
AgTob-NC **2b** (1:4.5:2:6 Ag:TMC:Tob:DS)	215.7 ± 1.36	0.238 ± 0.009	+13.3 ± 1.3	Tob: 76.5 ± 5.2% Ag: >95%

Fig. 2. Characterization of antimicrobial-functionalized NCs. (**A**) Hydrodynamic diameter (D_h, Z_{avg}), polydispersity index (PDI), surface charge, and ee% measurements for NC formulations, with varying ratios of Tob, DS, AgNPs, and TMC. Tob-NC **1c** was used to fabricate AgTob-NCs. Both NC **2a** and **2b** demonstrated near-quantitative loading of AgNPs with a 1:2 mass ratio of Ag:Tob. NC **2b** was functionalized with an additional 2.5 equivalent of TMC to create positively charged particles. (**B**) Scanning electron microscopy (SEM) image of **2a**. (**C**) SEM image of **2b**. Scale bars, 2 μm. (**D**) Tob-NC design parameters with Tob:DS-dependent trends for NC size and Tob ee%. (**E**) AgTob-NC design parameters for TMC-dependent NC size and charge.

10-nm AgNPs were chosen for LbL functionalization of Tob-NCs, as we hypothesized that this size would allow for formation of a thin layer on the particle surfaces and have been previously shown to have improved antimicrobial activity when compared to AgNPs of larger size (*14*). Trimethyl chitosan (TMC) was chosen as the positively charged polyelectrolyte to facilitate LbL loading of AgNPs onto NCs (Fig. 1A). TMC is a positively charged polysaccharide (Fig. 1D), which is biocompatible and has mucoadhesive properties, making it particularly attractive for applications in both oral and pulmonary drug delivery (*42–44*). In addition, chitosan and its derivatives have been shown to have antibacterial activities and enhance antibiotic efficacy (*45, 46*). TMC was first incubated with negatively charged AgNPs (ζ = −29.0 ± 1.15 mV) at a mass ratio of 1:1 to initiate complexation and form positively charged AgNPs (ζ = +17.4 ± 0.55 mV). TMC-coated AgNPs were then added to Tob-NCs to form AgTob-NCs, and additional TMC was added to stabilize the particles and prevent aggregation. Using this method at Na acetate (pH 4), quantitative loading of AgNPs onto NCs was observed, with tunable mass ratios of Ag:Tob ranging from 1:2 to 1:8. A ratio of 1:2 Ag:Tob was chosen to maximize loading and synergistic antimicrobial activities. The immediate addition of AgNPs to freshly formed Tob-NCs led to a 50- to 100-nm decrease in particle diameter (Fig. 2, A and E). This phenomenon is likely due to the strong electrostatic attraction between TMC and DS, as has been observed previously (*44*). This strong complexation also led to an increase in overall Tob ee% for AgTob-NCs, increasing from 58% for Tob-NC **1c** to >75% ee% for all AgTob-NCs fabricated.

In addition to coloading AgNPs and Tob onto a singular nanocarrier, we were interested in modulating the physicochemical properties of these NCs to design their biointerfacial interactions with bacterial biofilms. Because PA biofilms are composed of negatively charged biopolymers such as DNA and alginate, we hypothesized that positively charged NCs of a 200- to 300-nm size regime could initiate interactive filtering within biofilms (*29, 38*), with their size enabling steric diffusion through biofilm hydrogel pores while still allowing for electrostatic engagement with the biofilm matrix to increase NC attachment and antimicrobial delivery. To create positively charged AgTob-NCs, additional equivalents of TMC were added following AgNP coincubation. These studies yielded two different NC formulations, AgTob-NC **2a** bearing a negatively charged surface of −39.2 ± 1.5 mV and AgTob-NC **2b** with a positively charged surface of +13.3 ± 1.3 mV (Fig. 2, A and E). Both NCs **2a** and **2b** had similar degrees of Tob ee%, with **2b** being of slight increased size, likely because of the additional TMC layers coating its surface.

Storage, stability, and biocompatibility of AgTob-NCs

AgTob-NCs **2a** and **2b** were evaluated for their long-term storage potential, stability in biological environments, and biocompatibility. Both NC **2a** and **2b** were able to be lyophilized and resuspended without observable aggregation or destabilization, although a slight increase in particle size to ~300 nm in diameter was observed upon resuspension (fig. S2). To determine whether the NCs would destabilize or aggregate in biological medium, NCs were incubated in 10% fetal bovine serum for 20 hours at 37°C before characterization via DLS. NC **2a** maintained its size, and no aggregation was observed, while **2b** increased in size to ~1 μm (fig. S2) likely because of modest aggregation of NCs through the adsorption of serum

proteins onto the positively charged particle surfaces. PrestoBlue cell viability studies were performed using A549 lung cells incubated with AgNPs or NCs for 24 hours. AgNPs can be cytotoxic at higher concentrations (47, 48); however, we observed only modest decreases in cell viability to ~85% with AgNPs or NCs **2a** and **2b** at the highest dosage tested of 4 μg of AgNP per 20,000 cells, with no significant differences measured between groups (fig. S3). Thus, AgTob-NCs demonstrated favorable properties for long-term storage, stability, and biocompatibility.

Antimicrobial activity of AgTob-NCs against planktonic PA
With both NC formulations in hand, we set out to evaluate whether NC-mediated codelivery of Ag and Tob provided improved antimicrobial activity against planktonic cultures of PA. Laboratory strain PA14 was used for all antimicrobial activity assays, as PA14 is a well-studied virulent PA strain and can be cultured to form robust biofilms (49, 50). Tob, AgNPs, and AgTob-NC **2a** and **2b** were cultured with dilute concentrations of PA for 20 hours to determine the minimum inhibitory concentration (MIC) of Tob required to inhibit 80% of planktonic bacterial growth for each group relative to untreated PA14 cultures (Fig. 3).

Tob alone had an MIC value of 8 μg/ml, which is in agreement with the range commonly reported in the literature (13, 51). When coupled with AgNPs either coincubated in solution (AgNP + Tob control) or coloaded into NCs **2a** and **2b**, an enhancement in antimicrobial activity was observed, with Tob MIC values decreasing to 2 μg/ml (Fig. 3). AgNPs alone had an MIC value of 4 μg/ml, leading to a fractional inhibitory concentration (FIC) index value of 0.5, confirming synergistic activity as defined by an FIC of ≤0.5 (52). No significant differences were observed between any of the Ag + Tob treatment groups. Thus, NCs **2a** and **2b** delivered both antimicrobials effectively without sacrificing drug potency and enhanced the inhibition of planktonic PA growth when compared to Tob or AgNP treatments alone.

Antimicrobial activities of AgTob-NCs against PA biofilms
Because the majority of PA infections exists as biofilms that are associated with high rates of antimicrobial tolerance, we next evaluated the antimicrobial activities of AgTob-NCs against PA14 biofilms.
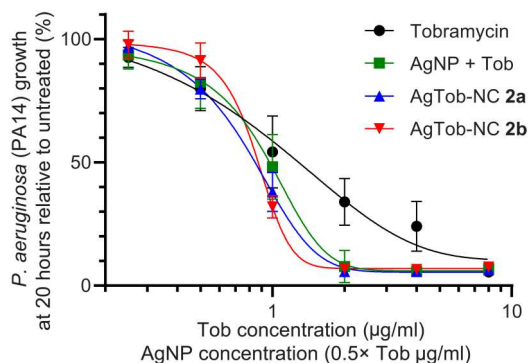

Fig. 3. Antimicrobial activity of AgTob-NCs against planktonic PA cultures. PA14 laboratory strains were incubated with Tob, AgNPs + Tob, or AgTob-NC formulations for 20 hours while shaking before measuring bacterial growth at an optical density at 600 nm (OD_{600}). The MIC_{80} of Tob decreased from 8 to 2 μg/ml with AgTob-NC treatment, demonstrating effective codelivery and synergistic enhancement in antimicrobial activity.

Biofilms were cultured for 24 hours using previously reported protocols before the addition of therapeutics and further incubation for 20 hours (50). PA14 biofilms were stained using a BacLight live/dead bacterial stain, with Syto9 acting as a universal stain for all bacteria and propidium iodide (PI) as a stain for dead bacteria with permeable membranes. PA14 grew into robust biofilms that displayed substantial antimicrobial tolerance to Tob, even at higher dosages of 40 μg/ml, corresponding to 6.4 μg of Tob per well (Fig. 4A). AgNP treatment alone also demonstrated no observable antimicrobial activity or reduction in biomass (figs. S4 and S5).

While neither Tob nor AgNP treatments alone could reduce biomass or cause reductions in bacterial viability, both AgTob-NCs **2a** and **2b** treatments led to observable changes in biofilm morphologies and significant reductions in bacterial biomass (Fig. 4B). Images were further quantified to determine the ratios of Syto9/PI fluorescence intensity as a marker for bacterial viability. Both NCs **2a** and **2b** led to significant bacterial growth inhibition and increases in membrane permeability when compared to Tob treatment alone, with NC **2b** leading to the most pronounced enhancement in antimicrobial activity (Fig. 4C).

Because the predominant difference between NC formulations was in the increased TMC coating and positive charge of NC **2b**, we sought to elucidate the influence of surface charge on the distribution of NCs within PA biofilms, as we hypothesized that the positively charged NC **2b** would have increased interactions with the negatively charged biofilm extracellular matrix. Fluorescein isothiocyanate–conjugated DS (FITC-DS) was used to fabricate fluorescent Tob-NCs with similar properties as Tob-NC **1c** (FITC-Tob-NC Z_{avg} $D_h = 271.7 \pm 2.2$ nm, $\zeta = -42.4 \pm 0.87$ mV). FITC-labeled Tob-NCs were then used to fabricate fluorescent NCs **2a** and **2b** and were added onto PA14 biofilms for 1 hour before analysis of NC-biofilm interactions via confocal fluorescence microscopy (Fig. 5). Microscopy analysis revealed that NC **2b** occupied more than twice the space within biofilms when compared to NC **2a** (Fig. 5C), and this increase in biofilm distribution likely led to enhanced antimicrobial activity.

Antimicrobial activity of AgTob-NCs in mouse models of lung infection
After determining the efficacy of AgTob-NCs in inhibiting bacterial growth in vitro, we next tested the antimicrobial activity of NC **2b** drug carriers in mouse models of lung infection. Wild-type C57BL/6 mice were anesthetized under isoflurane for 10 min and then intratracheally instilled with phosphate-buffered saline (PBS), Tob, or AgTob-NC **2b**. After 2 hours, the mice were anesthetized again with isoflurane and challenged via intratracheal instillation with 2×10^6 colony-forming units (CFUs) of PA14 per animal and monitored for survival outcomes over 24 hours. This model of NC installation and equilibration interval was chosen to model inhaled antibiotic therapies in patients with CF, which precede active exacerbations and are used as maintenance therapies while the patients are well to prevent further bacterial growth and subsequent complications. This 2-hour equilibration interval also allowed the mice to recover from anesthesia before bacterial installation. Physiologic measurements of temperature and weight change were taken every 2 hours after instillation, and no mice needed to be excluded on the basis of the Institutional Animal Care Use for Research Committee (IACUC) protocol for postprocedural weight loss. Treatment with PBS control before infection led to median survival of 8 hours, with
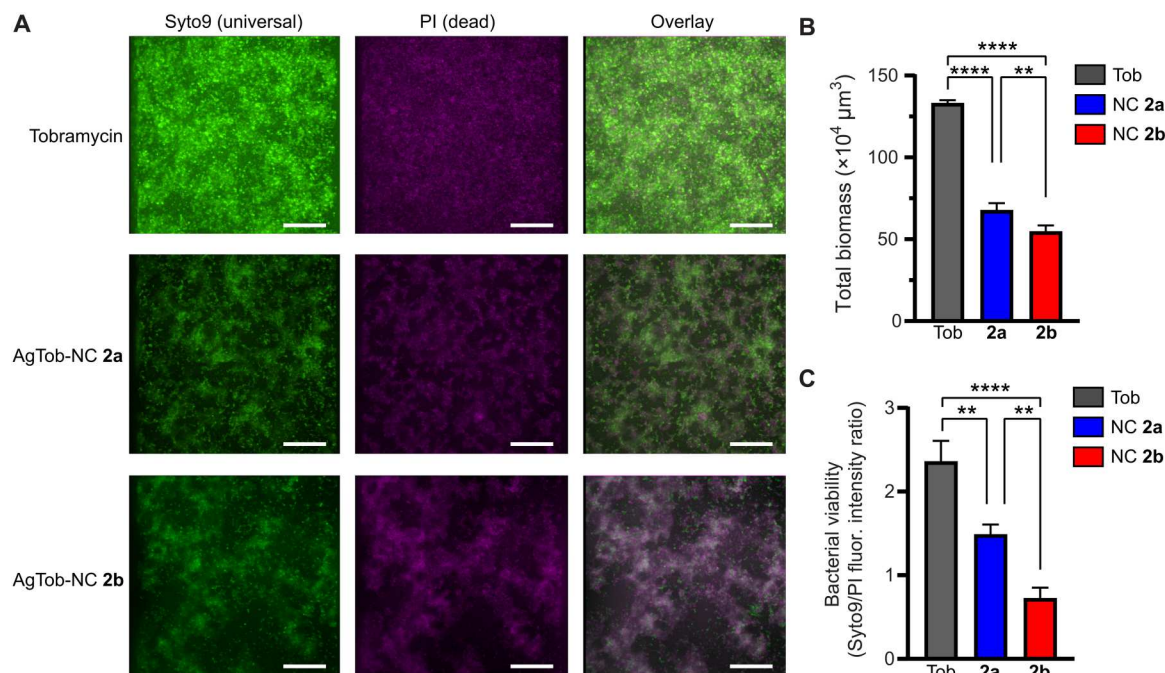
Fig. 4. Antimicrobial activities of AgTob-NCs against PA biofilms. (**A**) Representative three-dimensional (3D) projections of confocal fluorescence microscopy images of PA14 biofilms treated with Tob, AgTob-NC **2a**, or AgTob-NC **2b**. All biofilms were treated with 6.4 μg of Tob and/or 3.2 μg of AgNP for 20 hours. Syto9 (green) is a universal stain for both live and dead bacteria, while PI (magenta) stains only dead bacteria. White indicates overlay at approximately equal fluorescence intensities. Scale bars, 25 μm. Images were obtained at ×40 magnification. (**B** and **C**) Quantification of biofilm images to determine (B) biofilm biomass volumes and (C) bacterial viability as measured through the ratio of Syto9/PI intensities. Both NCs **2a** and **2b** led to biomass reduction and biofilm growth inhibition when compared to Tob-treated biofilms, with NC **2b** demonstrating the most pronounced effects. Image quantification was performed using ×20 magnification images. **$P < 0.01$; ****$P < 0.0001$. Additional images of biofilms treated with all groups and controls at ×20 magnification are available in the Supplementary Materials.

0 of 9 mice surviving the course of the study (Fig. 6A). When treated with Tob, survival outcomes increased to 3 of 8, while NC **2b** led to the highest survival rates of 8 of 10 mice ($P = 0.0004$). Temperature analysis of mice revealed body temperature decreases of approximately 12°C for the PBS-treated group, whereas Tob and NC treatments led to temperature decreases of approximately 5°C over the course of the study (fig. S6).

To quantify the bacterial burden of mice during the early stage of infection, mice were euthanized at 6 hours after infection, and CFU and physiological markers of infection were assessed. Total CFU counts combined from both bronchoalveolar lavage (BAL) and lung homogenization revealed that NC treatment reduced bacterial burden by ~1.5–log fold to levels of near clearance when compared to PBS control ($P = 0.0026$; Fig. 6B). Although no statistically significant differences were observed for white blood cell (WBC) count or weight gain between groups (fig. S7), NC treatment did reduce total protein levels from BAL compared to PBS control ($P = 0.0024$; Fig. 6C) while also limiting body temperature decreases over 6 hours ($P = 0.0063$; Fig. 6D). Histological analysis of lung sections after euthanasia at 6 hours revealed decreased neutrophilic inflammation and lung injury as measured by interstitial edema and disruption of the alveolar epithelial barrier in NC-treated mice (Fig. 6, E and F). For all quantitative metrics of infection, no statistical differences were observed between Tob and PBS treatment groups. Together, these studies demonstrate that NC therapy was the most effective treatment at reducing bacterial burden and physiological markers of infection and inflammation and increased overall survival outcomes.

DISCUSSION

Rising rates of antimicrobial-resistant bacterial infections and antimicrobial tolerant biofilms, coupled with limited approval of new antibiotics have led to a global crisis and fears of entering a postantibiotic era. It is therefore imperative to develop drug carrier formulations capable of enhancing the activities of already approved antibiotics such as Tob. By combining polyelectrolyte nanocomplexation with LbL electrostatic self-assembly, we developed a class of nanoscale drug carrier, capable of codelivering Tob antibiotics with antimicrobial AgNPs. While this drug combination had been previously reported in the literature for enhanced antimicrobial activity against PA biofilms (*14*), to our knowledge, it had not been tested in a nanoscale drug delivery formulation or in an in vivo model of infection.

Effective dual delivery of antimicrobials is particularly important for the treatment of bacterial biofilms, as insufficient antimicrobial delivery at sublethal doses can enhance biofilm growth (*53*, *54*). We observed that Tob and AgNP individual treatments led to greater biofilm formation when compared to untreated biofilm controls (fig. S5). This further highlights the need to develop nanocarrier formulations capable of interfacing with bacterial biofilms to deliver combination therapeutics and improve the efficacy of antimicrobials.
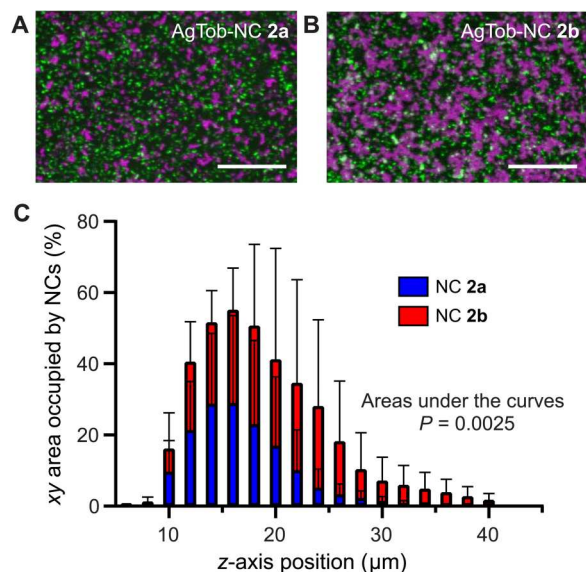
Fig. 5. Distribution of fluorescently labeled AgTob-NCs within PA14 biofilms. (**A** and **B**) Representative 3D projections of confocal fluorescence microscopy images of FITC NCs (magenta) within biofilms (green). Images were acquired 1 hour after NC addition to biofilms. Scale bars, 50 μm. (**C**) Quantification of biofilm images to determine % *xy* area occupied by FITC NCs within biofilms at each *z* position. Areas under the curves were calculated (307.7 ± 88.08 for NC **2a** and 745.3 ± 68.80 for NC **2b**), and $P = 0.0025$ was calculated by an unpaired *t* test.

The drug delivery method developed here led to high encapsulation rates of both Tob and AgNPs into the NC formulation while simultaneously allowing for physicochemical engineering of particle size and surface charge. These parameters are critical for the navigation of particles through biological barriers such as bacterial biofilms (*29*). NCs **2a** and **2b** were developed to match the reported pore sizes of biofilms. As bacterial biofilms are composed of negatively charged biopolymers such as polysaccharides and DNA (*2*), we hypothesized that positively charged NC **2b** would have strong electrostatic interactions with the biofilm matrix, enhancing the engagement and permeation of NC drug carriers throughout the biofilm via interactive filtering. In comparison, we hypothesized that negatively charged NC **2a** would quickly penetrate through the biofilm matrix or only locate to larger water channels within the biofilm hydrogel because of the electrostatic repulsion between NC **2a** and the negatively charged biofilm matrix. When observing NC distribution within established PA biofilms, we observed that NC **2b** occupied more than double the space as **2a** after 1 hour of incubation (Fig. 5). This increase in distribution likely contributed to the enhanced antimicrobial activity of NC **2b** when compared to **2a** (Fig. 4). While both NCs could release their payloads as determined in the planktonic MIC assays (Fig. 3) and lead to an inhibition in bacterial growth in biofilms when compared to Tob treatment alone (Fig. 4), NC **2b** had increased permeation into the PA biofilm to better deliver both Ag and Tob throughout the biomass, leading to greater reduction in both biomass and bacterial biofilm viability when compared to NC **2a**. These studies underscore the importance of drug carrier biointerface design (*29*), as these considerations can affect therapeutic outcomes.

Following in vitro studies, we set out to evaluate the therapeutic potential of NCs to clear PA lung infections in vivo. AgTob-NCs were evaluated in lung infection models as PA infections are prevalent in the lungs of patients with CF, where they are notoriously recalcitrant, requiring prolonged antibiotic treatment at high doses, which, even then oftentimes, does not prevent reinfection (*7*). Because NC **2b** demonstrated improved antimicrobial activities when compared to **2a** in our biofilm studies, it was selected for therapeutic evaluation in mouse models of lung infection to characterize the effects of NCs on preventing an ensuing lung infection. While no model perfectly captures the acute-on-chronic nature of bacterial CF lung infections, we based our model on the current gold standard of human therapies. Specifically, patients with CF are treated with inhaled antibiotics continuously for 1 month at a time to prevent PA exacerbations (*5, 7*). In addition to biofilm permeation properties, the additional coatings of TMC on NC **2b** surfaces could allow for increased bioadhesion and local retention, as TMC and other chitosan derivatives have been shown to have broad cyto- and mucoadhesive properties (*35*). For the model developed for these studies, therapeutics were administered intratracheally 2 hours before infection. When compared to other commonly used mouse models of lung infection where therapeutics and bacteria are coadministered simultaneously or in quick succession (*20, 21, 55*), this approach tests the sustained effects of therapeutics following administration (*5, 7*).

Using this model of lung infection, we observed that NC **2b** reduced bacterial burdens and improved survival outcomes to 80% when compared to PBS and Tob treatments, which had 0 and 37.5% survival outcomes, respectively (Fig. 6). As our model led to a median survival of 8 hours without antibiotic intervention, mice were euthanized at 6 hours to quantify bacterial burden at a relatively early time point within the spread of infection. This provided us with a holistic viewpoint of both the overall outcomes of treatment using the survival study and insight into the antimicrobial activities and biocompatibilities of Tob and NC **2b** using our 6-hour euthanasia model. While Tob treatment did not differ significantly from PBS in terms of reducing bacterial burden at 6 hours, NC **2b** treatment led to near complete clearance of bacterial load within the lungs. Some Tob-treated mice did display low bacterial load; however, the wider distribution of bacterial load within the Tob treatment group suggests that Tob treatment effects were heterogeneous when compared to NC delivery. The NC-improved bacterial reduction likely contributed to the 80% survival outcomes of NC treatment. Furthermore, NC **2b** treatment led to a reduction in BAL protein levels at 6 hours, indicating reduced lung injury. This finding agrees with histology images, wherein NC-treated lungs had reduced inflammation and healthier alveolar structures when compared to PBS- and Tob-treated lungs. Although no weight changes were observed between groups, this is likely due to the shorter 6-hour euthanasia time point, which would limit observable weight differences from the start of the study. Last, NC **2b** led to the greatest stability in body temperature when compared to PBS and Tob treatments, indicating that the NC treatment was well tolerated and effective in clearing bacterial lung infections.

These studies were limited to Tob treatment of PA, as PA is one of the most dominant bacterial species in CF lung infections and Tob is commonly prescribed for PA infections. However, the CF lung microenvironment oftentimes contains multiple bacterial species, which would require additional or alternative antibiotics
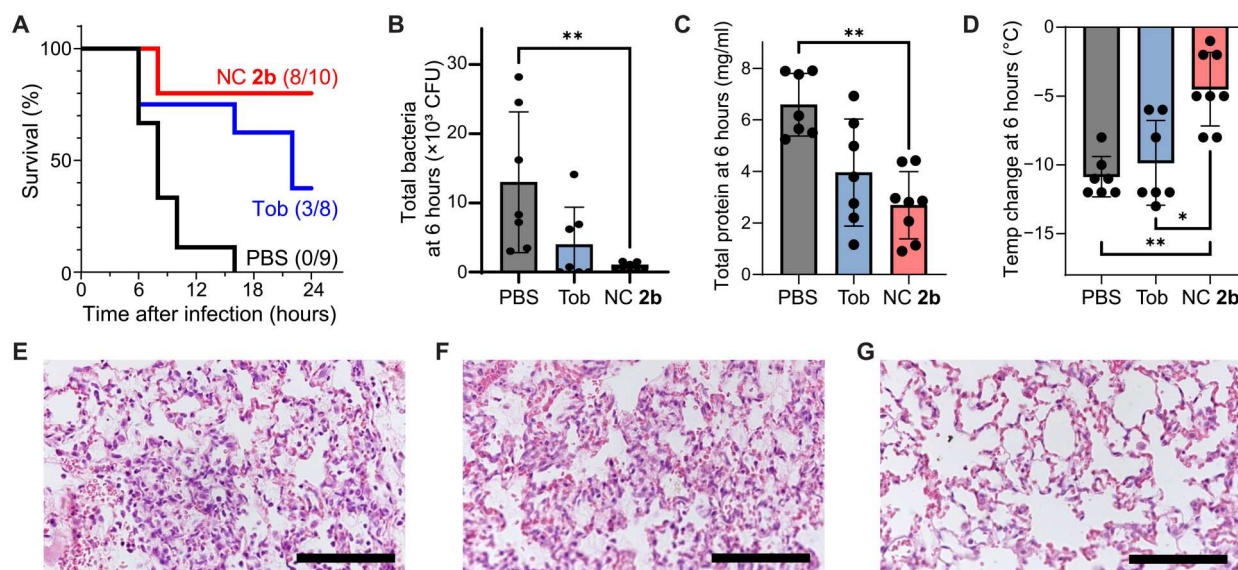
Fig. 6. Antimicrobial activity of AgTob-NCs in mouse models of lung infection. Wild-type mice were treated with Tob (0.2 mg/kg), AgTob-NC **2b**, or control (PBS) via intratracheal instillation for 2 hours before challenge with 2×10^6 CFUs of PA14. Mice were monitored for weight and temperature change and were either evaluated for survival over 24 hours or euthanized at 6 hours after challenge to quantify bacterial burden and physiological markers of infection. (**A**) Kaplan-Meier curve revealed improved survival outcomes in NC-treated mice, with 8 of 10 mice survival compared to 3 of 8 for Tob and 0 of 9 for PBS-treated groups, respectively ($P = 0.0004$). (**B**) Analysis of bacterial burden at 6 hours revealed that AgTob-NCs effectively reduced bacterial infection by approximately 1.5–log fold when compared to PBS control. (**C**) A reduction in BAL total protein count was determined in both Tob- and NC-treated mice. (**D**) Mice treated with NCs had reduced temperature decreases over 6 hours when compared to PBS or Tob treatments. (**E** to **G**) Representative images of hematoxylin and eosin–stained lung sections for (E) PBS-, (F) Tob-, and (G) NC-treated mice. Scale bars, 100 μm. For all graphs, *$P < 0.05$; **$P < 0.01$.

(*5, 7*). The NC-LbL strategies developed herein are highly versatile and could be applied toward other charged antibiotics such as gentamicin and polymyxins for use against both PA and other species present within mixed bacterial infections. In addition, the mucosal environment within CF lungs is highly viscous and poses a substantial delivery barrier, which would need to be addressed through codelivery of mucolytics with antimicrobials and further biointerface design of NC drug carriers to ensure mucosal diffusion while maintaining biofilm adhesion. The NCs in this study were administered via intratracheal instillation of a colloidal suspension, which could be adapted into a nebulizer for translational administration. Alternatively, the NC size, stability profiles, and ability to be lyophilized could enable their delivery via powder inhalation, as has been demonstrated for other nanoparticle formulations (*28*). This would increase the translational potential of AgTob-NCs and lead to their incorporation into an inhaler device similar to the commercially available Tobi Podhaler.

In summary, the NC-LbL antimicrobial formulation strategy developed in these studies led to the fabrication of tunable NCs and facilitated the codelivery of Tob and Ag to treat PA in both planktonic and antimicrobial tolerant biofilm states and improved therapeutic outcomes in mouse models of PA lung infection. By engineering the physicochemical properties of the NCs, we observed how surface chemistry influenced particle biointerfaces and resultant antimicrobial activities. Overall, this approach shows promise in the codelivery of diverse classes of antimicrobials to treat bacterial infections, including the recalcitrant biofilms associated with CF lung infections.

MATERIALS AND METHODS
General methods and instrumentation
Unless otherwise noted, all reagents were purchased from commercial sources. Low–molecular weight TMC was purchased from Sigma-Aldrich (St. Louis, MO) with a reported >70% degree of quaternization. Forty kilodalton DS with 15 to 19% sulfur content was purchased from Sigma-Aldrich (St. Louis, MO). Forty-kilodalton FITC-labeled DS was purchased from TdB Labs (Uppsala, Sweden), with 16 to 19% reported sulfur content. All reagent solutions were freshly prepared for each experiment and fabrication process. AgNPs of 10 nm in diameter were purchased from nanoComposix (San Diego, CA). Glycerol stocks of PA14 were provided by O. Rosenberg. A549 lung cells were provided by the UCSF Cell and Genome Engineering Core.

Zeta potential and DLS measurements were conducted on a Malvern Zetasizer Nano ZS. Absorbance and fluorescence quantification measurements were conducted on a Molecular Devices SpectraMax M5 plate reader. All fluorescence microscopy studies were conducted at the UCSF Nikon Imaging Center using a Nikon Ti spinning disk confocal microscope. Scanning electron microscopy (SEM) images were obtained at the UCSF Bioengineering and Biomaterials Correlative Imaging Core using a Zeiss Sigma 500 VP (Carl Zeiss Microscopy GmbH). All calculations and statistical analyses were performed using GraphPad Prism 9.2 software.

Tob-NC and AgTob-NC fabrication
Tob and DS were prepared as solutions (20 and 40 mg/ml) in double-distilled H_2O (ddH_2O), respectively. NC formation was accomplished through stepwise addition of DS, followed by Tob into a solution of 50 mM Na acetate (pH 4) for a final concentration of

Tob (2 mg/ml) and variable concentrations of DS to achieve mass ratios ranging from 1:1 to 1:4 Tob:DS. The solution was mixed by pipetting and left to incubate for at least 5 min before any subsequent reactions or characterizations.

For all AgTob-NC formulations, Tob-NCs were first fabricated at a 1:3 Tob:DS mass ratio. AgTob-NCs were typically fabricated at a 300-μl scale. Before fabrication, TMC [7.5 μl of 4 mg/ml in Na acetate (pH 4)] and AgNPs [30 μl of stock solution (1 mg/ml) obtained from commercial sources] were incubated together to achieve a 1:1 mass ratio. Next, a 75-μl solution of 0.05% (w/v) Tween 20 was prepared in ddH$_2$O, to which were added Tob-NCs (30 μl, 2 mg/ml), followed by the TMC-AgNP solution (37.5 μl). Additional TMC was then added as a 45-μl solution in ddH$_2$O (1 equivalent for NC **2a** and 3.5 equivalent for NC **2b**), followed by 60 μl of 5% (v/v) of poly(vinyl alcohol) (PVA) and 52.5 μl of ddH$_2$O to obtain AgTob-NCs as a 300-μl solution at Tob and Ag concentrations of 200 and 100 μg/ml, respectively. Tween 20 was used to prevent NC aggregation, while PVA was incorporated to enable the lyophilization of NCs for long-term storage. For all formulations developed, the amount of Tween 20 and PVA was kept consistent to avoid influence on particle morphology or drug loading efficiencies. AgTob-NCs were either used immediately or flash-frozen and lyophilized.

NC characterization and drug loading determination
DLS and zeta potential measurements were conducted using a Malvern Zetasizer Nano ZS. NCs were typically analyzed at a Tob concentration of 50 to 100 μg/ml. Particle hydrodynamic diameters (D_h) were reported using Z_{avg} measurements. Full DLS curves were obtained for intensity size distributions (fig. S2). ee% values for Tob were determined by analyzing the NC supernatants following centrifugation [13,000 rpm for 5 min] to evaluate drug depletion after NC formation and LbL AgNP loading. Centrifugation at this speed and time allowed for the formation of an NC pellet without pelleting AgNPs or Tob. AgNP depletion was analyzed via ultraviolet-visible absorbance at 390 nm, while Tob depletion was assessed via an o-phthalaldehyde fluorescence assay (37). Briefly, o-phthalaldehyde was prepared as a solution (1 mg/ml) in 100 mM Na borate (pH 10.4) buffer with the addition of methanol for 10% (v/v) and β-mercaptoethanol for 0.5% (v/v) final concentration. o-Phthalaldehyde solutions (15 μl) were added to isopropanol (90 μl) before the addition of sample supernatant (15 μl). Solutions were incubated for 20 min and then analyzed for fluorescence intensity (excitation/emission, 360/450) and compared to Tob calibration curves. o-Phthalaldehyde stock solutions could be stored at 4°C for 1 to 2 weeks without any observable loss in signal.

The morphology of the NC suspensions was determined using field-emission SEM (FE-SEM), Zeiss Sigma 500 VP (Carl Zeiss Microscopy GmbH). Samples for electron microscopy were prepared by mounting droplets of NC suspensions (20 μl) onto carbon substrate−coated SEM stubs and allowed to air dry. Subsequently, samples were stained with UranyLess. The UranyLess droplet was placed on the hydrophobic surface (parafilm). The stubs with NCs′ side were placed on the UranyLess drop for 2 min and thereafter blotted by filter paper to remove access stain on the NCs. Followed by washing three times with ddH$_2$O at room temperature. Last, the samples were dried at room temperature for at least 12 hours before analyzing via FE-SEM.

Mammalian cell culture and biocompatibility studies
A549 cells were cultured in F12 growth medium containing L-glutamine, supplemented with 10% fetal bovine serum and penicillin/streptomycin, and incubated at 37°C and 5% CO$_2$. For biocompatibility studies, A549 cells were trypsinized, resuspended to a concentration of 100,000 cells/ml, and plated in triplicate into a 96-well plate for a final cell number of 10,000 cells per well. After 24 hours of incubation, the medium was removed and replaced with 200 μl of medium + treatment (AgNP, AgTob-NC **2a**, or AgTob-NC **2b**). Treatments were prepared by fabricating the NCs as previously described at the Tob concentration of 200 μg/ml and the Ag concentration of 100 μg/ml in a final volume of 300 μl. This was further diluted into A549 medium for a final Ag concentration of 20 μg/ml, the highest concentration experimental condition. This was serially diluted 1:2 in A549 medium until reaching the Ag concentration of 0.625 μg/ml and added to the cells. The cells were then incubated for an additional 24 hours. Following incubation, 20 μl of PrestoBlue were added to each well. The cells were then incubated for 1 hour, and PrestoBlue fluorescence intensity (excitation/emission, 560/590) was measured to determine cell viabilities relative to untreated cells.

Planktonic PA antimicrobial activity studies
PA14 was cultured overnight from frozen glycerol stocks at 37°C and 220 rpm in LB medium. PA14 cultures were then refreshed by performing a 1:8 dilution into LB and shaken for an additional 1 to 3 hours until an optical density at 600 nm (OD$_{600}$) of >0.4 was achieved to confirm log phase bacterial growth. PA14 was then plated into 96-well plates at 100 μl and OD$_{600}$ = 0.002 in accordance with previously reported methods (56). Next, 100 μl of treatment groups and controls were added per well to achieve PA14 OD$_{600}$ = 0.001 and final treatment concentrations starting at 8 μg/ml for Tob and 4 μg/ml for Ag with 1:2 serial dilutions until a Tob concentration of 0.25 μg/ml and a Ag concentration of 0.125 μg/ml. All antimicrobial studies were performed with a minimum of n = 3 biological replicates. Plates were then incubated at 37°C and 220 rpm for 20 hours before measurement of OD$_{600}$ to assess bacterial viability relative to untreated controls. MIC values are defined as the minimum concentration of drug required to inhibit 80% bacterial growth relative to untreated controls.

PA biofilm studies
PA14 biofilms were grown using previously reported methods (50). PA14 overnight cultures were refreshed by performing a 1:8 dilution into LB and shaken for an additional 1 to 3 hours until an OD$_{600}$ of >0.4 was achieved to confirm log phase bacterial growth. Bacteria were then plated into half-area well plates (Greiner Bio-One) at 100 μl and OD$_{600}$ = 0.02 and sealed with air-permeable "Breathe-Easy" membranes. Plates were then placed into a stationary incubator with water bath and incubated at 37°C for 24 hours. After 24 hours, the air-permeable membranes were removed, and treatment groups were added to biofilms at 40 μl per well. Next, 20 μl of BacLight dyes Syto9 and PI (coincubated at 1:300 dilutions each from purchased stocks into PBS, following the manufacturer's instructions) were added to each well. Care was taken to add solutions dropwise to the top of each well without disturbing the biofilm. This addition afforded final Tob and Ag concentrations of 40 and 20 μg/ml, respectively, corresponding to 6.4 μg of Tob and/or 3.2 μg of Ag per well. After treatment and BacLight dye

addition, plates were sealed with air-permeable membranes and incubated at 37°C for 20 hours with gentle rotations at 50 rpm. After 20 hours, bacterial biofilms were imaged using confocal fluorescence microscopy, with Syto9 excited using a FITC channel and PI excited using a Cy3 channel. Images were acquired using both 20× and 40× air objectives. Images were acquired as z-stacks of biofilms, with 2-μm spacing and 50-μm total slices. z-stacks were centered at the z-position of highest Syto9 fluorescence intensity, and relative z-stacks were obtained ±25 μm from that slice. This image collection method afforded z-stacks of the entire biofilm. For NC distribution studies using fluorescently labeled NCs, all biofilm preparations and NC addition were performed as described above, as were image collection methods. However, biofilms were treated with 20 μl of CellTracker Red dye, prepared as a 1:200 dilution in PBS according with manufacturer instructions (Thermo Fisher Scientific) instead of Syto9 and PI. This allowed for visualization of biofilms in the Cy3 channel and visualization of NCs in the FITC channel. All biofilm studies were performed with a minimum of n = 3 biological replicates.

Biofilm image analysis and quantification

Image quantification of bacterial viability and biomass volume was done through ImageJ on biofilm z-stacks acquired with a 20× objective (xy pixel size of 512 by 512, corresponding to 240.6 μm by 240.6 μm, with 27 z slices). Of the slices obtained, slices 8 to 27 contained detectable biofilm signal and were used for all image analysis. The background was subtracted from all images within a stack, and the average fluorescence intensities of Syto9 and PI were then measured for each z slice. Syto9 fluorescence intensity and PI fluorescence intensity were averaged from all z slices, and a ratio of Syto9:PI fluorescence intensities was calculated. For biomass analysis, a background subtraction was performed, followed by a universal threshold determined on the basis of Otsu's binarization of the Syto9 channel in the untreated control biofilm. The % xy area occupied by biomass was measured for each z slice in a stack. This % area was then multiplied by the overall area of the field of view (59,707.6 μm^2) to calculate biomass area per z slice. A plot of "z-axis position (in micrometers)" versus "xy biomass area (in square micrometers)" was made, and the areas under the curves were calculated, which corresponded to total biomass volume in cubic micrometer. Total biomass volume and Syto9:PI ratios from three biological replicates were plotted as means ± SD. Statistical analysis was performed using one-way analysis of variance (ANOVA) with multiple comparisons (Tukey's method).

To quantify fluorescently labeled NC distribution within biofilms, background from each image was subtracted, followed by a universal threshold based on Otsu's binarization. The % xy area occupied by FITC NCs was measured for each z slice in a stack. A plot of z axis position (in micrometers) versus xy area occupied by NCs (in percentage) was made with means ± SD plotted for each z slice. Statistical analysis was performed by calculating the areas under the curves (745.3 ± 68.8 arbitrary unit (AU) for NC **2b** versus 307.7 ± 88.08 AU for NC **2a**) and conducting an unpaired t test on those values.

Care and use of mice

Mice were housed and bred in specific pathogen–free housing at the UCSF Laboratory Animal Research Center. All experiments were in accordance with the ethical principles and guidelines approved by

the UCSF IACUC approval number AN180640-03C. Eight- to 12-week-old male C57BL/6J wild-type mice were obtained from the Jackson Laboratory and used for lung infection studies. Pilot experiments with both female and male wild-type mice showed no difference between genders, and hence male mice were selected for this experiment.

Intratracheal PA models of lung infection

Mouse models of lung infection were performed according to established techniques (*49*). PA14 was streaked on plates from frozen glycerol stocks and a single colony selected for overnight culture at 37°C and 220 rpm in tryptic soy broth (TSB) medium. PA14 cultures were then refreshed the morning of infection by performing a 1:8 dilution into TSB and shaken for an additional 3 hours until an OD$_{600}$ of >0.4. Mice were randomly distributed into three groups (PBS, Tob, and NC treatments) and anesthetized with isoflurane before intratracheal instillation of therapeutics. Treatment groups were delivered at dosages of 0.2 mg/kg for Tob and 0.1 mg/kg for Ag in a total of 50 μl of injection volume. Mice were allowed to recover for 2 hours before isoflurane anesthetization and intratracheal instillation of 2×10^6 CFU of PA14 per animal in a volume of 50 μl. Animal weights and rectal temperatures were monitored every 2 hours for survival studies or at 6 hours before euthanasia for quantitative bacterial load and pathophysiology determination. To evaluate bacterial load at 6 hours, a BAL was performed before euthanasia and lung collection. BAL samples were used to determine BAL bacterial CFU, WBC numbers, and total protein levels. Lungs were homogenized in 1 ml of sterile PBS using sterile 100-μm filters and the sterile plunger from a 3-ml syringe. Fifty microliters of lung homogenate was then serially diluted and plated on *Pseudomonas* isolation agar (PIA) plates. CFU was calculated from dilution plates with 30 to 300 colonies, dividing the colony number by the dilution factor.

Total CFU was calculated by adding BAL and lung homogenate CFU counts. In the cases in which multiple dilution plates had 30 to 300 colonies, the average between plate counts was used. WBCs were measured by a hematology analyzer (Genesis, Oxford Science). Statistical analysis of survival studies was performed using a Mantel-Cox log rank test. Statistical analyses of quantitative metrics of bacterial infection and pathophysiology (CFU counts, WBC, total protein, weight change, and temperature change) were performed using Kruskal-Wallis nonparametric analyses with Dunn's correction for multiple comparisons. All statistics were performed using GraphPad Prism 9.

Supplementary Materials

This PDF file includes:
Figs. S1 to S7

View/request a protocol for this paper from *Bio-protocol*.

REFERENCES AND NOTES

1. P. Dadgostar, Antimicrobial resistance: Implications and costs. *Infect. Drug Resist.* **12**, 3903–3910 (2019).
2. H.-C. Flemming, J. Wingender, U. Szewzyk, P. Steinberg, S. A. Rice, S. Kjelleberg, Biofilms: An emergent form of bacterial life. *Nat. Rev. Microbiol.* **14**, 563–575 (2016).
3. I. Alav, J. M. Sutton, K. M. Rahman, Role of bacterial efflux pumps in biofilm formation. *J. Antimicrob. Chemother.* **73**, 2003–2020 (2018).

4. B. S. Tseng, W. Zhang, J. J. Harrison, T. P. Quach, J. L. Song, J. Penterman, P. K. Singh, D. L. Chopp, A. I. Packman, M. R. Parsek, The extracellular matrix protects *Pseudomonas aeruginosa* biofilms by limiting the penetration of tobramycin. *Environ. Microbiol.* **15**, 2865–2878 (2013).

5. I. D'Angelo, C. Conte, M. I. La Rotonda, A. Miro, F. Quaglia, Improving the efficacy of inhaled drugs in cystic fibrosis: Challenges and emerging drug delivery strategies. *Adv. Drug Deliv. Rev.* **75**, 92–111 (2014).

6. M. Facchini, I. De Fino, C. Riva, A. Bragonzi, Long term chronic *Pseudomonas aeruginosa* airway infection in mice. *J. Vis. Exp.* **85**, 51019 (2014).

7. O. Ciofu, T. Tolker-Nielsen, P. Ø. Jensen, H. Wang, N. Høiby, Antimicrobial resistance, respiratory tract infections and role of biofilms in lung infections in cystic fibrosis patients. *Adv. Drug Deliv. Rev.* **85**, 7–23 (2015).

8. K. B. Hisert, S. L. Heltshe, C. Pope, P. Jorth, X. Wu, R. M. Edwards, M. Radey, F. J. Accurso, D. J. Wolter, G. Cooke, R. J. Adam, S. Carter, B. Grogan, J. L. Launspach, S. C. Donnelly, C. G. Gallagher, J. E. Bruce, D. A. Stoltz, M. J. Welsh, L. R. Hoffman, E. F. McKone, P. K. Sing, Restoring cystic fibrosis transmembrane conductance regulator function reduces airway bacteria and inflammation in people with cystic fibrosis and chronic lung infections. *Am. J. Respir. Crit. Care Med.* **195**, 1617–1628 (2017).

9. H. Wu, C. Moser, H.-Z. Wang, N. Høiby, Z.-J. Song, Strategies for combating bacterial biofilm infections. *Int. J. Oral Sci.* **7**, 1–7 (2014).

10. S. Antoniu, Novel inhaled combined antibiotic formulations in the treatment of *Pseudomonas aeruginosa* airways infections in cystic fibrosis. *Expert Rev. Anti Infect. Ther.* **13**, 897–905 (2015).

11. A. Sabnis, K. L. Hagart, A. Klöckner, M. Becce, L. E. Evans, R. C. D. Furniss, D. A. Mavridou, R. Murphy, M. M. Stevens, J. C. Davies, G. J. Larrouy-Maumus, T. B. Clarke, A. M. Edwards, Colistin kills bacteria by targeting lipopolysaccharide in the cytoplasmic membrane. *eLife* **10**, e65836 (2021).

12. Z. Pang, R. Raudonis, B. R. Glick, T.-J. Lin, Z. Cheng, Antibiotic resistance in *Pseudomonas aeruginosa*: Mechanisms and alternative therapeutic strategies. *Biotechnol. Adv.* **37**, 177–192 (2019).

13. H. Ghorbani, M. Y. Memar, F. Y. Sefidan, M. Yekani, R. Ghotaslou, In vitro synergy of antibiotic combinations against planktonic and biofilm *Pseudomonas aeruginosa*. *GMS Hyg. Infect. Control* **12**, Doc17 (2017).

14. M. B. Habash, M. C. Goodyear, A. J. Park, M. D. Surette, E. C. Vis, R. J. Harris, C. M. Khursigara, Potentiation of tobramycin by silver nanoparticles against *pseudomonas aeruginosa* biofilms. *Antimicrob. Agents Chemother.* **61**, e00415–e00417 (2017).

15. J. Kim, B. Pitts, P. S. Stewart, A. Camper, J. Yoon, Comparison of the antimicrobial effects of chlorine, silver ion, and tobramycin on biofilm. *Antimicrob. Agents Chemother.* **52**, 1446–1453 (2008).

16. M. K. Rai, S. D. Deshmukh, A. P. Ingle, A. K. Gade, Silver nanoparticles: The powerful nanoweapon against multidrug-resistant bacteria. *J. Appl. Microbiol.* **112**, 841–852 (2012).

17. Q. Guo, T. Lan, Y. Chen, Y. Xu, J. Peng, L. Tao, X. Shen, Enhanced antibacterial activity of antibiotic-functionalized silver nanocomposites with good biocompatibility. *J. Mater. Sci. Mater. Med.* **30**, 34 (2019).

18. J. Hatzenbuehler, T. J. Pulling, Diagnosis and management of osteomyelitis. *Am. Fam. Physician* **84**, 1027–1033 (2011).

19. P. V. Baptista, M. P. McCusker, A. Carvalho, D. A. Ferreira, N. M. Mohan, M. Martins, A. R. Fernandes, Nano-strategies to fight multidrug resistant bacteria-"A battle of the titans". *Front. Microbiol.* **9**, 1441 (2018).

20. J. M. V. Makabenta, A. Nabawy, C.-H. Li, S. Schmidt-Malan, R. Patel, V. M. Rotello, Nanomaterial-based therapeutics for antibiotic-resistant bacterial infections. *Nat. Rev. Microbiol.* **19**, 23–36 (2021).

21. P. P. Kalelkar, M. Riddick, A. J. García, Biomaterial-based antimicrobial therapies for the treatment of bacterial infections. *Nat. Rev. Mater.* **7**, 39–54 (2022).

22. C. Deusenbery, Y. Wang, A. Shukla, Recent innovations in bacterial infection detection and treatment. *ACS Infect. Dis.* **7**, 695–720 (2021).

23. B. Porsio, M. G. Cusimano, D. Schillaci, E. F. Craparo, G. Giammona, G. Cavallaro, Nano into micro formulations of tobramycin for the treatment of *Pseudomonas aeruginosa* infections in cystic fibrosis. *Biomacromolecules* **18**, 3924–3935 (2017).

24. A. Nabawy, J. M. Makabenta, S. Schmidt-Malan, J. Park, C.-H. Li, R. Huang, S. Fedeli, A. N. Chattopadhyay, R. Patel, V. M. Rotello, Dual antimicrobial-loaded biodegradable nanoemulsions for synergistic treatment of wound biofilms. *J. Control. Release* **347**, 379–388 (2022).

25. D. Alkekhia, P. T. Hammond, A. Shukla, Layer-by-layer biomaterials for drug delivery. *Annu. Rev. Biomed. Eng.* **22**, 1–24 (2020).

26. M. Potter, A. Najer, A. Klöckner, S. Zhang, M. N. Holme, V. Nele, J. Che, L. Massi, J. Penders, C. Saunders, J. J. Doutch, A. M. Edwards, O. Ces, M. M. Stevens, Controlled dendrimersome nanoreactor system for localized hypochlorite-induced killing of bacteria. *ACS Nano* **14**, 17333–17353 (2020).

27. C. S. Schneider, Q. Xu, N. J. Boylan, J. Chisholm, B. C. Tang, B. S. Schuster, A. Henning, L. M. Ensign, E. Lee, P. Adstamongkonkul, B. W. Simons, S.-Y. S. Wang, X. Gong, T. Yu, M. P. Boyle, J. S. Suk, J. Hanes, Nanoparticles that do not adhere to mucus provide uniform and long-lasting drug delivery to airways following inhalation. *Sci. Adv.* **3**, e1601556 (2017).

28. S. Haque, M. R. Whittaker, M. P. McIntosh, C. W. Pouton, L. M. Kaminskas, Disposition and safety of inhaled biodegradable nanomedicines: Opportunities and challenges. *Nanomedicine Nanotechnol. Biol. Med.* **12**, 1703–1724 (2016).

29. J. A. Finbloom, F. Sousa, M. M. Stevens, T. A. Desai, Engineering the drug carrier biointerface to overcome biological barriers to drug delivery. *Adv. Drug Deliv. Rev.* **167**, 89–108 (2020).

30. Z. Zhao, A. Ukidve, V. Krishnan, S. Mitragotri, Effect of physicochemical and surface properties on in vivo fate of drug nanocarriers. *Adv. Drug Deliv. Rev.* **143**, 3–21 (2019).

31. V. V. Sheffey, E. B. Siew, E. E. L. Tanner, O. Eniola-Adefeso, PLGA's plight and the role of stealth surface modification strategies in its use for intravenous particulate drug delivery. *Adv. Healthc. Mater.* **11**, 2101536 (2022).

32. Y. Wang, A. Shukla, Bacteria-responsive biopolymer-coated nanoparticles for biofilm penetration and eradication. *Biomater. Sci.* **10**, 2831–2843 (2022).

33. K. W. Kolewe, S. R. Peyton, J. D. Schiffman, Fewer bacteria adhere to softer hydrogels. *ACS Appl. Mater. Interfaces* **7**, 19562–19569 (2015).

34. A. E. Marras, J. M. Ting, K. C. Stevens, M. V. Tirrell, Advances in the structural design of polyelectrolyte complex micelles. *J. Phys. Chem. B* **125**, 7076–7089 (2021).

35. D. Wu, L. Zhu, Y. Li, X. Zhang, S. Xu, G. Yang, T. Delair, Chitosan-based colloidal polyelectrolyte complexes for drug delivery: A review. *Carbohydr. Polym.* **238**, 116126 (2020).

36. A. D. Kulkarni, Y. H. Vanjari, K. H. Sancheti, H. M. Patel, V. S. Belgamwar, S. J. Surana, C. V. Pardeshi, Polyelectrolyte complexes: Mechanisms, critical experimental aspects, and applications. *Artif. Cells Nanomedicine Biotechnol.* **44**, 1615–1625 (2016).

37. M. Hill, R. N. Cunningham, R. M. Hathout, C. Johnston, J. G. Hardy, M. E. Migaud, Formulation of antimicrobial tobramycin loaded PLGA nanoparticles via complexation with AOT. *J. Funct. Biomater.* **10**, 26 (2019).

38. J. Witten, K. Ribbeck, The particle in the spider's web: Transport through biological hydrogels. *Nanoscale* **9**, 8080–8095 (2017).

39. S. Correa, E. C. Dreaden, L. Gu, P. T. Hammond, Engineering nanolayered particles for modular drug delivery. *J. Control. Release* **240**, 364–386 (2016).

40. D. Alkekhia, A. Shukla, Influence of poly-l-lysine molecular weight on antibacterial efficacy in polymer multilayer films. *J. Biomed. Mater. Res. A* **107**, 1324–1339 (2019).

41. J. A. Finbloom, B. Demaree, A. R. Abate, T. A. Desai, Networks of high aspect ratio particles to direct colloidal assembly dynamics and cellular interactions. *Adv. Funct. Mater.* **30**, 2005938 (2020).

42. S. Ahadian, J. A. Finbloom, M. Mofidfar, S. E. Diltemiz, F. Nasrollahi, E. Davoodi, V. Hosseini, I. Mylonaki, S. Sangabathuni, H. Montazerian, K. Fetah, R. Nasiri, M. R. Dokmeci, M. M. Stevens, T. A. Desai, A. Khademhosseini, Micro and nanoscale technologies in oral drug delivery. *Adv. Drug Deliv. Rev.* **157**, 37–62 (2020).

43. A. D. Kulkarni, Y. H. Vanjari, K. H. Sancheti, H. M. Patel, V. S. Belgamwar, S. J. Surana, C. V. Pardeshi, New nasal nanocomplex self-assembled from charged biomacromolecules: *N,N,N*-trimethyl chitosan and dextran sulfate. *Int. J. Biol. Macromol.* **88**, 476–490 (2016).

44. A. D. Kulkarni, H. M. Patel, S. J. Surana, Y. H. Vanjari, V. S. Belgamwar, C. V. Pardeshi, *N,N,N*-trimethyl chitosan: An advanced polymer with myriad of opportunities in nanomedicine. *Carbohydr. Polym.* **157**, 875–902 (2017).

45. Z. Si, Z. Hou, Y. S. Vikhe, K. R. V. Thappeta, K. Marimuthu, P. P. De, O. T. Ng, P. Li, Y. Zhu, K. Pethe, M. B. Chan-Park, Antimicrobial effect of a novel chitosan derivative and its synergistic effect with antibiotics. *ACS Appl. Mater. Interfaces* **13**, 3237–3245 (2021).

46. S. A. Agnihotri, N. N. Mallikarjuna, T. M. Aminabhavi, Recent advances on chitosan-based micro- and nanoparticles in drug delivery. *J. Control. Release* **100**, 5–28 (2004).

47. C. Liao, Y. Li, S. C. Tjong, Bactericidal and cytotoxic properties of silver nanoparticles. *Int. J. Mol. Sci.* **20**, 449 (2019).

48. T. Zhang, L. Wang, Q. Chen, C. Chen, Cytotoxic potential of silver nanoparticles. *Yonsei Med. J.* **55**, 283–291 (2014).

49. J. Qu, N. K. Prasad, M. A. Yu, S. Chen, A. Lyden, N. Herrera, M. R. Silvis, E. Crawford, M. R. Looney, J. M. Peters, O. S. Rosenberg, Modulating pathogenesis with MOBILE-CRISPRi. *J. Bacteriol.* **201**, e00304-19 (2019).

50. M. Müsken, S. Di Fiore, U. Römling, S. Häussler, A 96-well-plate-based optical method for the quantitative and qualitative evaluation of Pseudomonas aeruginosa biofilm formation and its application to susceptibility testing. *Nat. Protoc.* **5**, 1460–1469 (2010).

51. R. M. Shawar, D. L. MacLeod, R. L. Garber, J. L. Burns, J. R. Stapp, C. R. Clausen, S. K. Tanaka, Activities of tobramycin and six other antibiotics against *Pseudomonas aeruginosa* isolates from patients with cystic fibrosis. *Antimicrob. Agents Chemother.* **43**, 2877–2880 (1999).

52. C. D. Doern, When does 2 plus 2 equal 5? A review of antimicrobial synergy testing. *J. Clin. Microbiol.* **52**, 4124–4128 (2014).

53. L. R. Hoffman, D. A. D'Argenio, M. J. MacCoss, Z. Zhang, R. A. Jones, S. I. Miller, Aminoglycoside antibiotics induce bacterial biofilm formation. *Nature* **436**, 1171–1175 (2005).

54. A. Tahrioui, R. Duchesne, E. Bouffartigues, S. Rodrigues, O. Maillot, D. Tortuel, J. Hardouin, L. Taupin, M. C. Groleau, A. Dufour, E. Déziel, G. Brenner-Weiss, M. Feuilloley, N. Orange, O. Lesouhaitier, P. Cornelis, S. Chevalier, Extracellular DNA release, quorum sensing, and PrrF1/F2 small RNAs are key players in *Pseudomonas aeruginosa* tobramycin-enhanced biofilm formation. *NPJ Biofilms Microbiomes* **5**, 15 (2019).

55. C. Cigana, S. Ranucci, A. Rossi, I. De Fino, M. Melessike, A. Bragonzi, Antibiotic efficacy varies based on the infection model and treatment regimen for *Pseudomonas aeruginosa*. *Eur. Respir. J.* **55**, 1802456 (2020).

56. R. Agarwal, C. T. Johnson, B. R. Imhoff, R. M. Donlan, N. A. McCarty, A. J. García, Inhaled bacteriophage-loaded polymeric microparticles ameliorate acute lung infections. *Nat. Biomed. Eng.* **2**, 841–849 (2018).